Obscure Variables in Battery Research: Impacts of Spacer Thickness and Slurry Formulation Protocols

Maxwell Gao

A thesis

submitted in partial fulfillment of the

requirements for the degree of

Master of Science

University of Washington

2025

Committee:

Jun Liu

Mitchell Kaiser

Program Authorized to Offer Degree:

Materials Science & Engineering

University of Washington

Abstract

Obscure Variables in Battery Research: Impacts of Spacer Thickness and Slurry Formulation Protocols

Maxwell Gao

Chair of the Supervisory Committee:

Jun Liu

Department of Materials Science & Engineering

Abstract – While much battery research focuses on new materials and full-cell designs, early-stage battery evaluation still relies on small, lab-scale coin cells, where often-overlooked factors can significantly affect test results. This work investigates two critical yet underexamined aspects of electrode performance: cell pressure and slurry formulation. First, the impact of spacer thickness, and thus internal cell pressure, on the electrochemical performance of sodium-ion coin cells is examined using hard carbon anodes. Findings show that insufficient compression leads to unstable contact, reduced capacity, and greater variability, while greater compression promotes higher capacity and greater cycle stability. Theories explaining these findings are discussed. Second, the optimization process of aqueous slurry mixing for hard carbon electrodes is presented. The sources of particle agglomeration and slurry inconsistency are found, ultimately developing a reliable protocol that improves coating uniformity and slurry stability.

1. Introduction

1.1. Background

As the need to make society's energy from renewable means becomes increasingly an urgent task, batteries play a key role in circumventing one of renewable sources' typical flaws: intermittency. By storing generated energy in a way that can be released as needed on the grid-scale, the reliance on carbon-emitting power plants can be drastically reduced.[1] In parallel, the continued development of batteries is enabling more and more technologies to transition from fossil fuels to electric power – including ground vehicles, watercraft, and aircraft.

These emerging applications, especially in high-performance and safety-critical areas, are placing increasingly tall demands on battery systems. Although they were initially developed for consumer electronics, lithium-ion batteries (LIBs) now play a pivotal role in enabling all of these technologies and must deliver a variety of greater metrics, such as higher energy and power densities, faster charging, stable operation across wider temperature ranges, and maintaining greater thermal and mechanical stability.

Different applications also demand different metrics. For example, electric vehicles demand high energy density and fast charging comparable to the range and refueling speed of gas-powered cars, all while meeting strict safety standards. Aviation, meanwhile, imposes even greater constraints, requiring extremely high volumetric and gravimetric energy and power densities, uncompromising safety, and reliable performance under extreme temperatures.

To meet these diverse demands, the field of battery research has expanded into a wide array of directions – including novel materials, cell design, electrode architecture, and scalable manufacturing methods. Unfortunately, achieving multiple performance targets simultaneously is far from straightforward**,** as improvements in one metric often come with trade-offs in another. For instance, increasing energy density may reduce safety margins or cycle life, while optimizing electrodes for manufacturability might compromise performance.

Compounding these issues is the fact that while much attention is being given to novel materials and full-scale battery integration, less emphasis is placed on how those electrodes and cells are tested. Nearly all battery research begins with small, lab-scale tests involving coin cells, the testing of which lacks standardization.[3] Subtle differences in parameters such as spacer thickness, compression, or slurry and coating quality can lead to significant variation in electrochemical results, undermining research reproducibility and interpretability. Rather than rigidly enforcing standardized test setups, a more powerful approach is to understand how each step – from slurry mixing to electrode coating to cell assembly – contributes to the final electrode quality and performance. This approach not only makes comparisons across studies more contextualized, but also improves the clarity, reliability, and reproducibility of battery research itself. Additionally, this will help bridge the gap between ambitious performance goals and early-stage lab research by optimizing and accurately assessing electrode testing environments, thereby making lab testing more reflective and predictive of high-performance capabilities.

In particular, hard carbon has emerged as a promising anode for both sodium and lithium-ion batteries due to its potential for higher capacity, lower voltage, and higher rate capability compared to graphite. Its performance is highly sensitive to processing conditions, especially in aqueous slurries, where control of slurry behavior and particle dispersion are generally less forgiving than NMP-based slurries.[4][5] Therefore, to realize and accurately assess the potential of this material, understanding how to consistently produce and test these electrodes is imperative. While this work focuses on the use of hard carbon, the emphasis on the electrode fabrication and coin-cell testing steps will be applicable to many other systems.

1.2. Research Scope

This work focuses on improving the practice of lab-scale battery research. While the field continues to expand the frontiers of novel materials and large-scale deployment, there remains a critical need to deepen our understanding of overlooked details in lab-scale research and how

they influence observed performances. This work will therefore consist of two projects. First, the effect of spacer thickness/internal cell pressure on coin cell performance is investigated in a hard carbon/sodium system. Next, several aqueous slurry mixing strategies are employed to improve electrode qualities, and successful strategies are discussed to better understand particle and slurry behavior.

2. Material/Equipment Sources and General Methods

2.1. Material and Equipment Sources

Commercial hard carbon on aluminum electrodes were purchased from MTI Corporation (SKU = bcaf-BHCss). Hard carbon was purchased from Kuraray (9 μm, type 2), MTI Corporation (SIB-BHC400), or MSE Supplies (MSE PRO Hard Carbon). Sodium metal on aluminum chips were purchased from MTI Corporation. Polypropylene (PP) separators were purchased from Celgard (3501). Glass fiber separators were purchased from Cytiva (Whatman GF/A and GF/F). $NaPF_6$ was purchased from Oakwood Chemicals, and DME was purchased from Gotion.

All cell parts were purchased from MTI to produce 2032 coin cells, including the anode and cathode case, the stainless steel spacers (thicknesses = 0.5, 1.0 mm), and the stainless steel spring. Carbon-coated aluminum foil, the doctor blade, and the electrode coater were purchased from MTI. The battery cycler used was manufactured by Neware.

2.2. General Methods

All electrodes were punched into 13 mm diameter discs using handheld cutters from Beyond Battery (SKU = CNA7-10-12 and CNA7-10-13) to form coin cell electrodes. All separators were punched into 19 mm discs using handheld cutters from Beyond Battery (SKU = CNA7-10-19) or MTI Corporation (MSK-T-10). All materials were dried under vacuum at the following temperatures before quickly transferring to the glovebox: Electrodes, glass fiber separators, coin cell parts, and lithium/sodium salts were dried in the vacuum oven at 100°C overnight, while plastic separators were dried at 60°C–70°C overnight. Solvents that were shipped packaged under argon were directly transferred into the glovebox. 1M $NaPF_6$ in DME

was prepared by dissolving .16795g of the salt in 1000µL of DME, measured using an analytical scale and micropipette. Volume change from dissolving salt was assumed to be negligible.

2.3. General Half Coin Cell Production

All coin cells were produced by layering the components in the following order and crimped using a MTI MSK-110 Hydraulic Crimping Machine at 50 kg/m^2 inside an argon-filled glovebox by VacuumTechnologyInc: the anode case, the punched electrodes, ½ of the total electrolyte volume, one or more separators, the remaining ½ of the electrolyte volume, a sodium metal on aluminum or lithium metal chip, one or more stainless steel spacers, a stainless steel wave spring, and finally, the cathode case (**Figure 1**). All spacers were placed with the lip/sharp edges facing up. Each coin cell of the same type and cycling condition was produced 3 times for consistency in each experiment, unless otherwise stated.

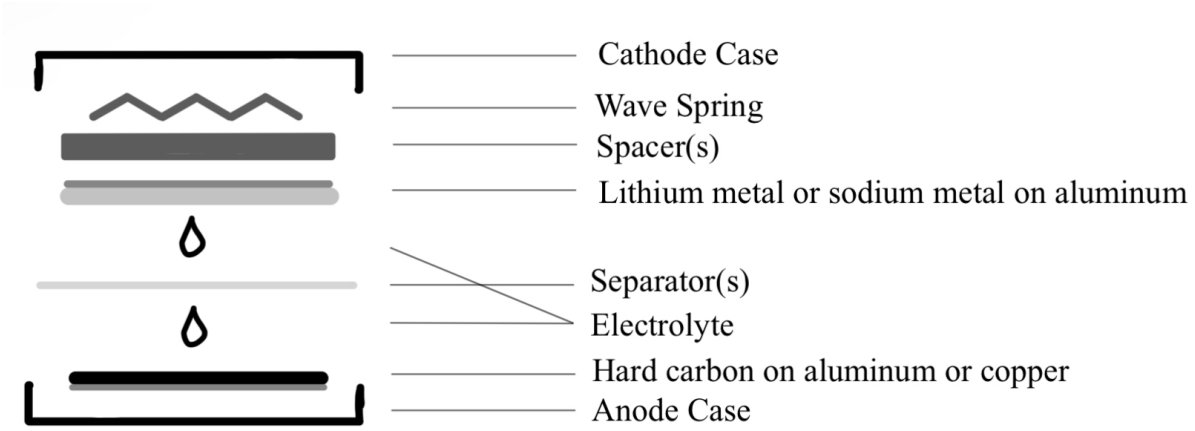

Figure 1. Half-coin cell assembly diagram.

3. Cell Pressure Project

3.1. Methods

Half cells were produced using commercial hard carbon electrodes (diameter = 13 mm) against sodium metal on aluminum chips with 100 µL of 1M $NaPF_6$ in DME. Three separators were used to ensure no dendrite penetration: a PP separator, a glass fiber (GF/F type) separator, followed by another PP separator. In this experiment, the second aliquot of electrolyte was added after the glass fiber separator was added, but before the second PP separator was added to ensure good wetting of the glass fiber separator. Four types of cells were produced, each with a different number/thickness of spacers (thicknesses = no spacers, 0.5, 1.0, and 1.5 mm). Cells

with 1.5 mm thick spacers were made using a 1.0 mm and a 0.5 mm thick spacer, stacked in that order. Cells were cycled in a Neware cycler at 0.1 C for 3 cycles as formation cycles, followed by continuous cycling at 1 C.

To obtain estimates of spring compression, the thicknesses of 5 coin cells crimped at 50 kg/m^2 and the center of 5 anode and cathode coin cell cases were measured. The thicknesses of the PP separator, glass fiber separator, hard carbon electrode, and sodium on aluminum chip were taken from each manufacturer's claims (25, 420, 110, 450 μm, respectively) while the thicknesses of the 0.5 and 1.0 mm spacers were assumed to be 0.5 and 1.0 mm, respectively. To calculate the amount of free space for the spring, the average thickness of the 5 anode and cathode cases, along with the thicknesses of all other components (hard carbon electrode, 2x PP separators, glass fiber separator, spacer(s), and the sodium on aluminum chip), were subtracted from the average thickness of the 5 crimped coin cells. A low-end estimate of the standard deviation for the spring compression was found by square-rooting the sum of the variances for the thickness of each component if known, which included the cell thickness, anode case, cathode case, and stainless steel spring. For this estimate, the spring was assumed to be the only compressible component, making the compression distance a high-end estimate.

3.2. Results and Discussion

3.2.1. Voltage-capacity plots

The cells with no spacers indicated a high likeliness of soft-short circuiting or being unable to achieve good electrical contact, as seen by the small capacity and spikes in the voltage vs. capacity curves (**Figure 2**). One of the three assembled cells with no spacers showed sustainable operation, but that cell showed significantly worse capacity compared to all other working cells (Figure 1, cell 2). It is more likely that poor electrical contact is the main cause of the behaviors seen for several reasons: At this early stage, it is unlikely that enough lithium has been stripped to form a dendrite long enough to pierce the separators, especially all three separators that were used in these cells. This is further supported by the lower voltage of the discharge curve at cycle

1, indicating a significant source of resistance was formed in the circuit, which could be caused by a bottleneck for electron flow. This meant that a lower potential was needed to sustain the same lithiation rate, thereby hitting our cutoff voltage (.01V) before significant utilization of the hard carbon plateau region, leading to poor capacity. Finally, it is supported by spring compression estimates, which will be discussed later (**Table 1**). Any following discussion in this section will therefore assume this behavior to be indicative of poor electrical contact, although further study may be needed to fully validate this.

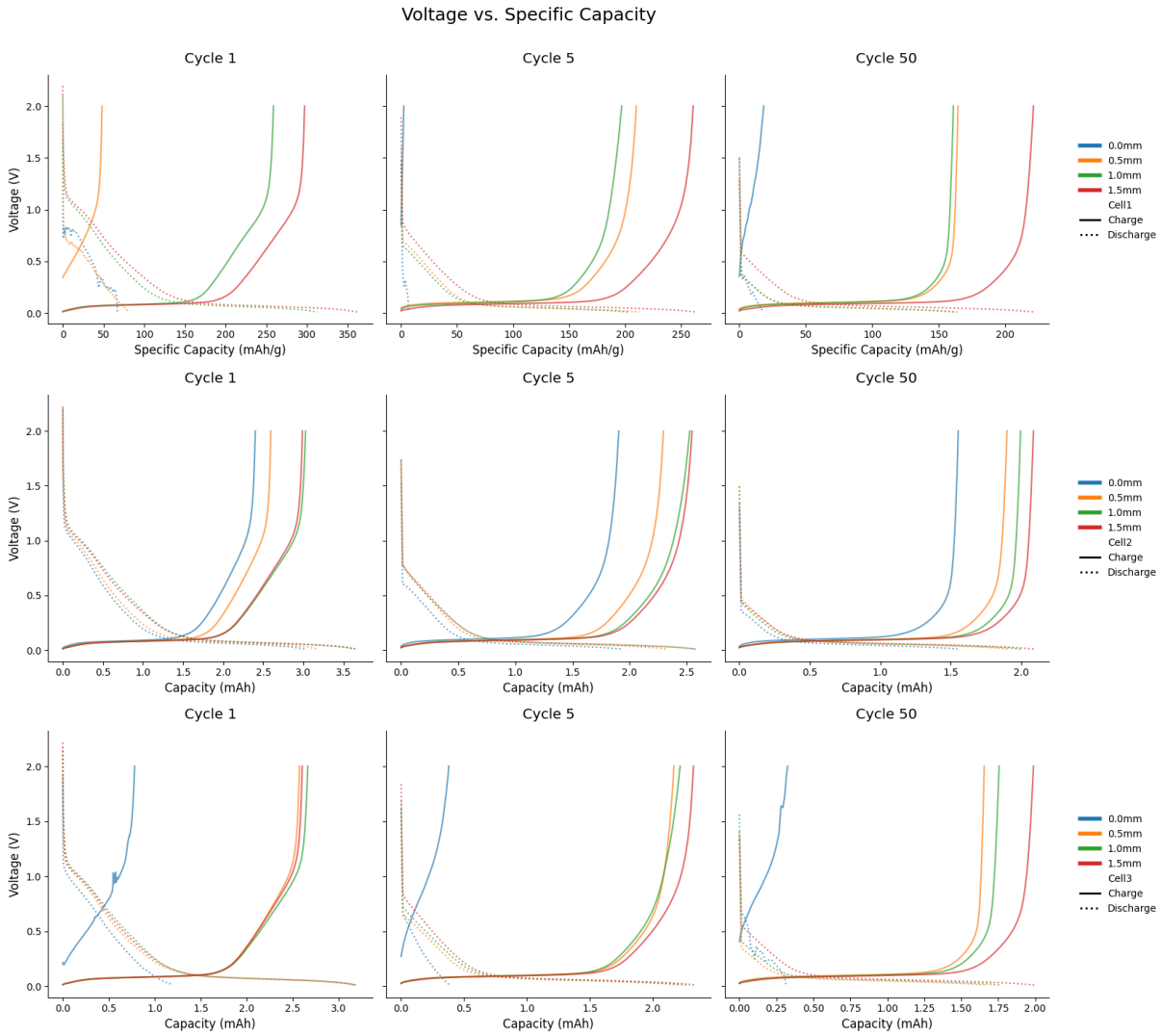

Figure 2. Voltage versus capacity plots of cycles 1, 5, and 50 for cells assembled using no spacers (blue), 0.5 mm thick (orange), 1.0 mm thick (green), and 1.5 mm thick (red) spacers. Charge/discharge curves are solid/dotted, respectively. C-rates were .1C for cycle 1, and 1C for cycles 5 and 50.

Of the three 0.5 mm spacer cells, one also occasionally showed poor electrical contact (example in cell 1, cycle 1), indicating no spacers and one 0.5 mm spacer are not thick enough to

guarantee good contact. These findings agree with the estimates of the spring compression and the standard deviation for the thicknesses of all components, discussed in the next section.

3.2.2. Spring compression estimates

Estimates for the distance of spring compression along with the standard deviation of the thicknesses of all cell parts, with and without the spring are shown in **Table 1**. Row 1 shows the amount of space left in the cell if there were no spring, i.e., the amount of space left for the spring to fill, while row 2 shows the distance the 1.2 mm spring is compressed. In cells with no spacers, there is free space left in the cell, even with a fully uncompressed spring, implying that there will be no or poor contact. Meanwhile in the 0.5 mm spacer cells, there is a small amount of compression. However, this compression distance is relatively large compared to the calculated standard deviation, which was a low-end calculation as it did not include the standard deviation for the thicknesses of the electrode, separators, or spacers. Additionally, because the spring is not the only compressible element in the system, the spring compression estimates are high-end estimates. Combined with the high standard deviation relative to the estimated spring compression, it is unsurprising to find a 0.5 mm spacer cell occasionally exhibiting poor electrical contact.

The 1.5 mm spacer cells had 0.135 mm of free space left for the spring, but the springs used were 0.3 mm thick when fully compressed. This may be a concern as it can indicate there is not enough space within the cell, even with a fully compressed spring. However, because the free space estimates are low-end estimates, the reality may be that other components are compressing to accommodate, such as the glass fiber separator.

Table 1. Estimates of free space and amount of spring compression in 2032 coin cells crimped at 50 kg/cm^2 with different spacer thicknesses and the combined standard deviation of the thicknesses.

	No Spacers	.5 Spacer	1.0 Spacer	1.5 Spacer	Standard Deviation
Leftover Space (No Spring)	1.635	1.135	0.635	0.135	0.021
Spring Compression	-0.435	0.065	0.565	1.065	0.054

It may be surprising to find that the cells with no spacers cycled at all, given that there should be about .435 mm of extra space in the cell, implying that there is no contact at all. However, there may be a good reason for this: the electrodes were prone to curling, which was easily noticeable after drying in the vacuum oven and after wetting with the first aliquot of electrolyte. While the cells were produced with the anode case facing down, the cells were cycled with the anode case facing up. This means that after flipping the coin cell, the weight would be removed from the electrode, and its tendency to curl may provide contact with the anode case (**Figure 3**).

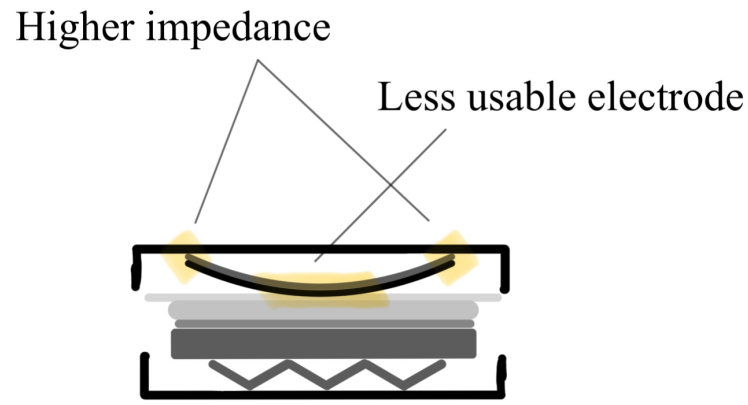

Figure 3. Areas of reduced contact (highlighted) in a cell where the electrode is curled, resulting in higher cell impedance and lowered usable area of electrode.

If this occurs, the area of contact between the electrode and anode case, as well as the electrode and separator/sodium will be reduced, causing two effects: a bottleneck for electron flow would be created, increasing cell impedance, and less electrode will be usable, causing reduced capacity. Variations in how much space is left and how much the electrode needs to curl in order to contact the anode case will affect the reduction in area of contact, creating different amounts of impedance and reductions in cell capacity (higher space/more curling = less contact area/higher impedance/lower capacity).

This curling can therefore explain the ability of the no spacer cells to cycle, as well as the increased impedance seen as a downward shift in the discharge voltage curve, and the significantly lowered capacity of the single well-functioning no spacer cell (Figure 2, cell 2).

These affects may also translate to the generally lower capacities of the 0.5 mm spacer cells as well, as contact in those cells is expected to be unstable as well.

3.2.3. Capacity versus cycling

It has been shown that pressure can improve cycle life in pouch cells, [2] and a similar effect may be seen here (**Figure 4**). This can be seen in the flattening of the capacity curve in the 1.5 and 1.0 mm spacer cells, whereas the 0.5 mm spacer cells continuously fell. While the 1.0 mm and 0.5 mm cells started off with similar capacities, the standard deviation fills clearly illustrate the 1.0 mm cells overtaking the 0.5 mm cells around cycles 40+.

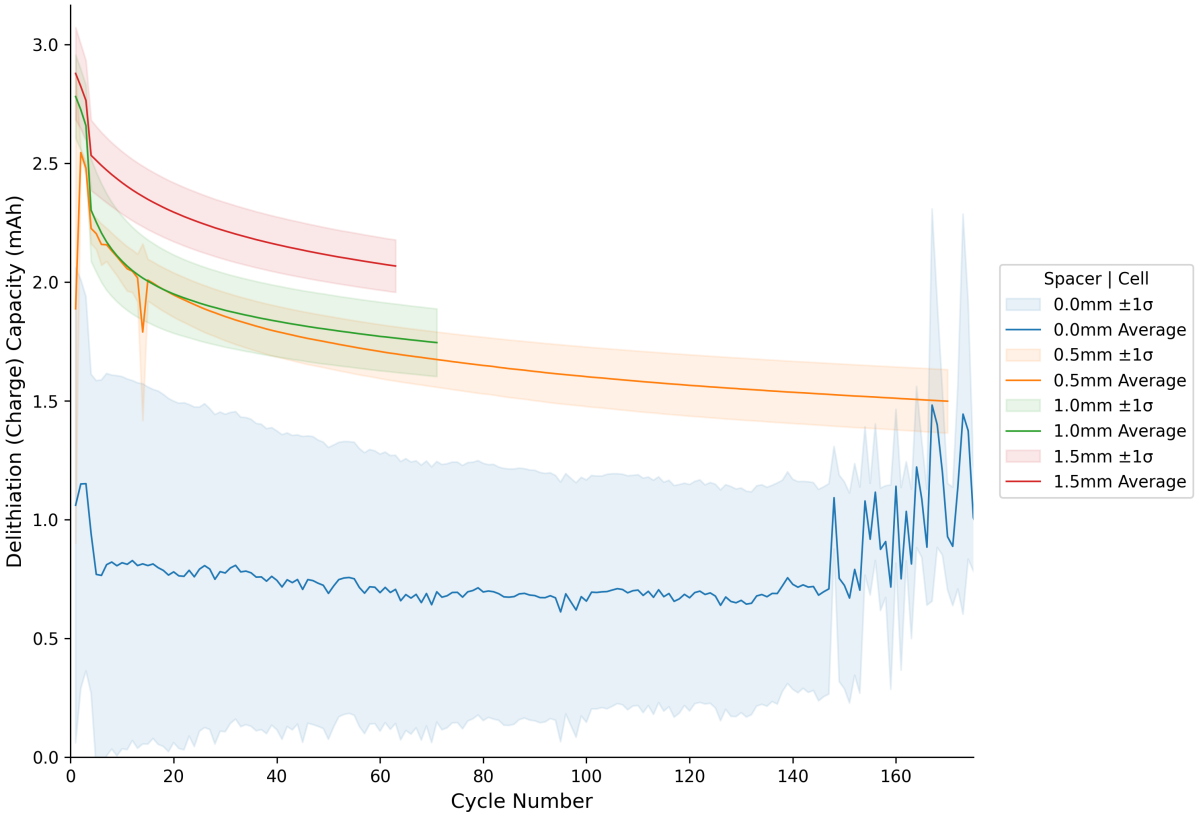

Figure 4. Average of the delithiation (charge) capacity versus cycle number for cells with no spacers (blue), 0.5 mm (orange), 1.0 mm (green), and 1.5 mm (red) spacers. Shaded fill represents the average ± the standard deviation.

Specifically, Figure 2 shows that this capacity degradation is caused by the shrinking of both the plateau region (0<V<.1) and the sloping region (V>.1). The former effect can be seen by comparing the sloping region between the cells in the 1st and 5th cycles, then at the 50th. In the discharging curve for all cells (excluding the no spacer cells) during the 1st cycle, the voltage drops to the sloping region at around ~1.2V, then steadily slopes towards ~.1V over the next

~1.5 mAh. The plateau region then begins, and the voltage is steady until full capacity. In cycle 5, a small difference begins to emerge. The higher the spacer thickness in the cell, the higher the voltage of the beginning of the sloping region. Compared to cycle 1, these voltages are lower, so it is more accurate to describe that the higher thickness cells exhibited a smaller drop in this initial sloping voltage. It is, however, important to note that cycle 5 was at a higher rate (1C) compared to cycle 1 (.1C), so the difference between these two cycles can also be an indication of lower rate capability of smaller spacer cells and is likely not entirely indicative of cycling degradation. Nonetheless, the difference between cycles 5 and 50 is more attributable to this effect. By cycle 50, the 0.5 mm and 1.0 mm spacer cells began the sloping region discharge at less than .5V, down from the ~.75V in cycle 5. On the other hand, only one of the 1.5 mm spacer cells began the discharge at <.5V, while the other two began at >.5V (Figure S1). This means that the voltage drops to .1V sooner for 0.5 and 1.0 mm spacer cells, leading to a smaller sloping capacity.

It is important to note that in the 1.5 mm spacer cells, there may be an effect attributable to the compression of the separators for the 1.5 mm spacer cells, which can reduce impedance by reducing ion diffusion distance. Further study will be needed to confirm if this has a significant effect. Finally, Figure 4 also shows instability in the capacity in the first 20 cycles of the 0.5 mm spacer cells, likely caused by the poor contact previously discussed. The instabilities in the no spacer cells can also be seen.

3.3. Conclusions

These results demonstrate that the use of different spacer thicknesses has a significant impact on the electrochemical performance of coin cells. Cells without spacers exhibited behaviors consistent with poor electrical contact, likely due to insufficient spring compression and curling of the electrode, which together contributed to high impedance and erratic/reduced capacity. While 0.5 mm spacers offered marginal improvement, they did not guarantee adequate contact across trials. In contrast, the 1.0 mm and 1.5 mm spacer cells exhibited more stable and higher

capacities over cycling, with the 1.5 mm configuration showing by far the greatest performance. These findings highlight the importance of mechanical consistency in lab-scale cell assembly and suggest that differences in cell internal pressure, although often overlooked, can introduce substantial variability in coin cell results. This reinforces the need for careful control and reporting of cell assembly parameters in early-stage battery research.

4.4. Future Works

Future work can improve on this by directly measuring internal cell pressure using pressure-sensitive films to better quantify the true mechanical compression experienced by the cell components. Additionally, investigating a wider range of spacer thicknesses, particularly between 1.0 and 1.5 mm, could help elucidate minor trends in pressure application, as all spacer thicknesses tested here had potential reasons to show different performances outside of just pressure effects (ex. separator compression). Different springs with different spring constants can also be investigated as another control point for tuning pressure application. These insights could contribute to standardizing coin cell assembly practices for improved reproducibility and contextualized results in battery research.

4. Slurry Optimization Project

4.1. Methods

Slurries of hard carbon were mixed according to various protocols, displayed in Table 2. Materials are prepared according to the material preparation column(s): The materials listed in the first column are loaded into a small Thinky mixer cup (Yamayu UG, 24 mL) and mixed according to the mixing step listed below the material list inside of a Thinky mixer at atmospheric pressure. The materials of the next column are then added and mixed according to the step listed in that column, and this is repeated for all columns listed. The slurry was then dropped onto carbon-coated aluminum foil adhered to a flat surface (glass, stainless steel, or aluminum) using ethanol, and an electrode coater was used to push a doctor blade to apply the slurry. The coating speed used was 8.0 (units unknown) and the doctor blade gap was set to 180 μm. All mixing and defoaming steps were performed at 2000 and 2200 rpm, respectively.

Medium (M), small (S), and tiny yttria-stabilized zirconia milling balls were respectively of diameters 3, 1, and .5 mm, and were purchased from MTI Corporation.

Table 2. All slurry mixing protocols. Bolded steps are key changes from the previous mixing protocol or important changes in the results.

	Material Preparation	Mixing Steps (Material Added Mixing/Defoam Time)			Result	Main Changes and Notes
Protocol 1	C45 and hard carbon (HC) are dried in the vacuum oven and stored in desiccator. Both materials sieved before use.	.1g C45, 2.5g CMC in H_2O (1.5%), 6M 20S Zr balls 20m mix	1.8g hard carbon, 1.6g H_2O 20m mix	.25g SBR in H_2O (25%) 5m mix, 3m defoam, 5m cooling	Large particles, slight bubbling	Original protocol
Protocol 2	**C45 grinded.** C45 and HC are dried in the vacuum oven and stored in desiccator. Both materials sieved before use.	.1g C45, 2.5g CMC in H_2O (1.5%), 6M 20 S Zr balls 20m mix	1.8g hard carbon, 1.6g H_2O 20m mix, **5m cooling, 20m mix**	.25g SBR in H_2O (25%) 5m mix, **10m defoam**, 5m cooling	Large Particles	Grind C45. Increased mixing and defoam time.
Protocol 3	C45 grinded. C45 and HC are dried in the vacuum oven and stored in desiccator. Both materials sieved before use.	**.05g** C45, **1.25g** CMC in H_2O (1.5%), 6M 20 S Zr balls 20m mix	**.9g** hard carbon, **.8g** H_2O 20m mix, 5m cooling, 20m mix	**.125g** SBR in H_2O (25%) 5m mix, 10m defoam, 5m cooling	Large Particles	Batch size halved.
Protocol 4	C45 grinded. C45 and HC are dried in the vacuum oven and stored in desiccator. **Only C45 sieved before use.**	.05g C45, 1.25g CMC in H_2O (1.5%), 6M 20 S Zr balls 20m mix	.9g hard carbon, .8g H_2O 20m mix, **5m sonication**, 20m mix	.125g SBR in H_2O (25%) 5m mix, 10m defoam, **5m sonication**	Large Particles	Replaced water cooling with sonication.
Protocol 5	**Premixed .075g C45 and 1.35g HC in mortar with 750µL H2O.**	**1.45g premix,** 1.25g CMC in H_2O (1.5%), 6M 20S Zr balls 20m mix, 5m sonication	**300µL H_2O** **10m mix, 20m defoam,** 20m mix, 5m defoam	**125µL** SBR in H_2O (25%) **5m mix, 3m defoam, 5m sonication**	Fewer particles	Pre-mixed C45 and HC with water. Used pipette for water and SBR.
Protocol 6	Premixed **.055g** C45 and **.99g** HC in mortar. **(No H_2O)**	**.95g** premix, 1.25g CMC in H_2O (1.5%), 6M 20S Zr balls **10m mix,** 5m sonication	**800µL** H_2O **20m mix**	125µL SBR in H_2O (25%) 5m mix, 3m defoam, 5m cooling	**Fewer particles. Slurry was runny.** Coating thickness range: **25-86** µm.	Pre-mixed C45 and HC without water. **Used CMC#5**.
Protocol 7	Premixed .055g C45 and .99g HC in mortar.	.95g premix, 1.25g CMC in H_2O (1.5%), No Zr balls 10m mix, 5m sonication	**500**µL H_2O, **6M 0S Zr balls** 20m mix	125µL SBR in H_2O (25%) 5m mix, 3m defoam, 5m cooling	**More particles**. **Slurry was runny.**	Removed Zr balls in initial mixing step and used less water. **Used CMC#5**.
Protocol 8	**Dried CMC before making solution.** Premixed .055g C45	.95g premix, 1.25g CMC in H_2O (1.5%), No Zr balls	**800µL** H_2O, 6M **20S** Zr balls	125µL SBR in H_2O (25%)	**Fewer particles.** Slurry was of	Removed all sonication steps, dried

	and .99g HC in mortar.	10m mix, **no sonication**	20m mix	5m mix, 3m defoam, 5m cooling		better consistency. Coating thickness range: **101-107** µm	CMC. **Coated directly on coating machine.**
Protocol 9	Dried CMC before making solution. Premixed .055g C45 and .99g HC in mortar.	.95g premix, 1.25g CMC in H2O (1.5%), No Zr balls **20m** mix	500µL H2O, 6M 20S Zr balls 20m mix	300µL H2O 20m mix	125µL SBR in H2O (25%) 5m mix, 3m defoam, 5m cooling	**Significantly reduced particles, for several months.**	Water addition broken into 2 steps. Increased initial mixing time.
Most Recent	**Milled, sieved, dried C45 before use and stored in glovebox.** Dried CMC before making solution. Premixed .055g C45 and .99g HC in mortar.	.95g premix, 1.25g CMC in H_2O (1.5%), No Zr balls 20m mix	500µL H_2O, 6M 20S Zr balls 20m mix	300µL H_2O 20m mix	125µL SBR in H2O (25%) 5m mix, 3m defoam, 5m cooling	Significantly reduced particles. **Slurry was of good consistency**.	C45 preparation and storing.

4.2. Rationale, Results and Discussion

4.2.1. Initial attempts and findings

This section will not only discuss the results of the mixing parameters on the coating result, but also explain the rationale behind the key changes between the protocols to give insight into the modification choices. Starting with the original protocol, Protocol 1: This was based off a protocol given by Kha Le at PNNL and simply modified to have double the batch size. Large particles/agglomerates and slight bubbling was seen in the electrode coat. The particles were suspected to be C45 particles, as during the sieving step, the C45 took a long time to fall through the sieve, whereas the hard carbon that was used during most of the slurry optimization process (Kuraray, 9µm, type 2) fell through with little effort. This indicated significant agglomeration in the C45, so in Protocol 2, the C45 was grinded in a mortar and pestle prior to sieving. To further break down agglomerates, an additional 20 min mixing was introduced after the second 20 min mixing step, separated by a 5 min cooling period to avoid excessive heat buildup. Defoaming time was also increased to remove bubbles, although it was discovered that the better optimization factor was not increasing defoaming time, but instead to avoid the introduction of bubbles when adding the CMC solution. Increased mixing time also appeared to have little effect on breaking down agglomerates.

In Protocol 3, the batch size was halved down to the original batch size given by Kha Le for consistency, which thereby also increased the ratio of milling balls to slurry content. This was suspected to give a higher chance for the milling balls to crush the agglomerates, but this had a minimal effect on the coat quality. Next, because sonication is known to be an effective measure in breaking down agglomerates, all water-cooling steps were replaced with sonication to simultaneously cool and preserve particle suspension in Protocol 4. Additionally, only C45 was sieved, as the hard carbon showed a consistently quick sieving process, indicating a consistent lack of agglomeration. This protocol still produced a fair number of large particles, so it became apparent that C45 could agglomerate even after grinding and sieving, and that sonication was insufficient to break the agglomeration that occurred.

4.2.2. Pre-mixing

A new strategy was then proposed, inspired by established SOPs from other slurry chemistries, which was to pre-mix the C45 with the hard carbon in a mortar. In theory, this would allow the C45 to adhere to hard carbon particles, which could prevent C45 from agglomerating with itself. This pre-mixing step was done with an aliquot of water in Protocol 5 and without the water in Protocol 6. Both procedures showed a noticeable reduction in the number of large particles. Little difference was seen between protocol 5 and 6, so the water-free pre-mixing step was used in subsequent procedures to avoid inconsistent water evaporation during this step, which will later affect the total amount of water added to the slurry. During the following protocols, sieving of any material was stopped.

4.2.3. Coating surface

Around this time, the thickness profile of each electrode was being recorded, and it was found that the thicknesses were highly ununiform throughout each electrode, thereby significantly varying mass loading. Thickness differences of over 20 μm between the thickest and thinnest parts of the electrode were found in every coat, sometimes ranging as high as 60 μm. All thickness measurements were taken ~1 cm away from any edge, and ~2 cm away from the

location the slurry was initially dropped to begin the coat to avoid non-uniformity from the electrode edges.

This issue was quickly fixed, as it was found that the coating surfaces used at the time (glass panes) had slight warping. Given that the coating gap ranged from 150-200 μm high, this warping had a huge effect on the coating uniformity. Starting in Protocol 8, the carbon-coated aluminum foil was adhered either directly to the stainless-steel platform on the electrode coater or on precision-machined aluminum plates. Subsequent electrode coats had coating ranges less than 10 μm, indicating the importance of an ultra-flat surface for a uniform coat and consistent mass loading.

4.2.4. Binder drying

Around the time of testing Protocol 6 and 7, it was observed that the slurry consistency was runny, and the problem was traced to the runny consistency of a particular batch of CMC solution. This batch was a noticeably thinner liquid compared to other batches of CMC, and remaking the solution yielded the same thin solution. Two things were attempted in protocols 7 and 8: reducing the addition of water in the slurry and drying the CMC in a vacuum oven overnight at 100°C to remove water and storing it in the glovebox. Reducing the water in the slurry did increase the viscosity, although a large viscosity difference was observed in very small (~50 μL) additions of water, indicating that binder content was low. Using dried CMC produced solutions and slurries of thicker consistency, indicating that storing CMC in a desiccator was insufficient to prevent moisture absorption. This would also explain the apparently low binder content, and could also contribute to the observed particle agglomeration, as binder is known to preserve particle suspension.

4.2.5. C45 preparation

In protocol 9, the above findings were consolidated into an established procedure, which worked for several months for all types of hard carbon (MTI, MSE, Kuraray). Unfortunately, particle agglomeration returned after, making it apparent that the storage method (desiccator),

drying, and pre-mixing, were insufficient. Therefore, by breaking agglomeration in the C45 and other materials and storing it in the glovebox, moisture adsorption can be prevented up until the particles are added into the slurry, by which point the binder will help preserve particle dispersion. The materials were prepared by an initial drying in vacuum oven (100°C, overnight), then by mixing ~0.5 g of the material in the Thinky mixer with ~3 g of small and ~ 7 g of tiny yttria-stabilized zirconia milling balls for 3 minutes. It was then scraped with a spatula to re-mix the particles with the milling balls, as the material formed a film-like compaction on the bottom of the container. This was repeated four times, and the powder was then sieved, re-dried in the vacuum oven, and then transferred into the glovebox. The powder easily fell through the sieve, even for C45 indicating good breakup of agglomeration.

This preparation method was used in the final, most up-to-date protocol, and successfully reduced agglomeration. It also noticeably increased slurry viscosity, which is expected as more particle-solvent interactions are formed.

4.3. Conclusions

In this study, a series of slurry mixing protocols were developed to reduce particle agglomeration and improve slurry consistency. Initially, agglomeration was addressed through grinding, sieving, and sonication, but it was found that the most effective measures were pre-mixing powders together, grinding and storing materials in the glovebox, and ensuring that binders were thoroughly dried before use. It was found that storing materials in the desiccator still allowed the materials to intake water, thereby increasing its mass or inducing agglomeration. Additionally, switching to coating on top of precision-machined surfaces instead of glass panes resulted in significant improvements in coating uniformity. These results show that there are numerous practices which influence electrode slurries, and that making a high-quality electrode is very challenging, requiring careful control of the material preparation and mixing processes.

4.4. Future Works

Rheological analysis can be used to quantify viscosity to be able to follow smaller trends in viscosity changes. By pairing this analysis with coating speed and doctor blade thicknesses, the relation between these parameters and the final electrode thickness can be investigated and be used as factors to predict mass loading. Additionally, further works can look to systematically optimize the mixing steps, as the effects of some mixing and defoaming times were convoluted with material preparation procedures, and it remains unclear if and how the mixing steps have an impact on the slurry. Changes in the formulation can also be studied on particle dispersion behavior, such as variations in the binder or conductive carbon content.

Acknowledgements

I would like to acknowledge Jun Liu for taking me into the lab as student and providing the equipment and materials to make these studies possible. Furthermore, I would like to thank Anthony Romero, Bhagyesh Trivedi, Minh Duong, Zhi Peng, and Trung Nguyen for the discussions which massively contributed to my understanding of battery systems, and Dr. Mitchell Kaiser for managing the lab. I would like to specifically thank Bella Wu for being my mentor, giving me guidance throughout these projects, and answering my incessant questioning. Lastly, I would like to thank everyone in the lab for being goofballs and preserving a fun, enriching learning environment.

References

[1] Shaner, M. R.; Davis, S. J.; Lewis, N. S.; Caldeira, K. Geophysical constraints on the reliability of solar and wind power in the United States (vol 11, pg 914, 2018). *Energ Environ Sci* **2018**, *11* (4), 997-997. DOI: 10.1039/c8ee90019a.

[2] Leonard, A.; Planden, B.; Lukow, K.; Morrey, D. Investigation of constant stack pressure on lithium-ion battery performance. *J Energy Storage* **2023**, *72*. DOI: ARTN 108422 10.1016/j.est.2023.108422.

[3] Stüble, P.; Müller, C.; Bohn, N.; Müller, M.; Hofmann, A.; Akçay, T.; Klemens, J.; Koeppe, A.; Kolli, S.; Rajagopal, D.; et al. From Powder to Pouch Cell: Setting up a Sodium-Ion Battery Reference System Based on $Na_3V_2(PO_4)_3$/C and Hard Carbon. *Batteries Supercaps* **2024**, *7* (12). DOI: ARTN e202400406 10.1002/batt.202400406.

[4] Reynolds, C. D.; Walker, H.; Mahgoub, A.; Adebayo, E.; Kendrick, E. Battery electrode slurry rheology and its impact on manufacturing. *Energy Adv* **2025**, *4* (1), 84-93. DOI: 10.1039/d4ya00380b.

[5] Reynolds, C. D.; Hare, S. D.; Slater, P. R.; Simmons, M. J. H.; Kendrick, E. Rheology and Structure of Lithium-Ion Battery Electrode Slurries. *Energy Technol-Ger* **2022**, *10* (10). DOI: ARTN 2200545 10.1002/ente.202200545.